PHYSICAL REVIEW B **95**, 161410(R) (2017)

Inelastic electron tunneling into graphene nanostructures on a metal surface

N. Néel,[1,*] C. Steinke,[2,3] T. O. Wehling,[2,3] and J. Kröger[1]
[1]*Institut für Physik, Technische Universität Ilmenau, D-98693 Ilmenau, Germany*
[2]*Bremen Center for Computational Materials Science, University Bremen, D-28359 Bremen, Germany*
[3]*Institute for Theoretical Physics, University Bremen, D-28359 Bremen, Germany*
(Received 27 February 2017; published 28 April 2017)

Wrinkles and blisters of graphene on Ir(111) give rise to remarkably high signals in inelastic electron tunneling spectroscopy due to graphene phonons. Spatially resolved spectra unravel the gradual increase of the graphene phonon signatures with progressive delamination of graphene from the metal surface. Spectroscopy of the Ir(111) surface resonance evidences that the graphene-metal hybridization is efficiently reduced in wrinkles and blisters. A high phonon density of states favors the observation of phonons with wave vectors near the $\overline{M}$ point of the surface Brillouin zone.

DOI: 10.1103/PhysRevB.95.161410

I. INTRODUCTION

While many laterally averaging spectroscopy methods have been used to explore graphene phonons and their dispersion [1–7], local inelastic electron tunneling spectroscopy (IETS) studies performed with a scanning tunneling microscope (STM) have scarcely been reported. Phonons of graphene on metal surfaces have not been unveiled with IETS, presumably due to the graphene-metal hybridization. Graphene on SiC [8], on SiO_2 [9,10], and on top of hexagonal boron nitride (hBN) on SiO_2 [11,12] was shown to exhibit inelastic signatures of graphene phonons in the spectra of the differential conductance (dI/dV). Remarkably, changes in dI/dV due to the excitation of graphene phonons were huge compared to the spectroscopy signatures of, e.g., molecular vibrations [13]. Moreover, the signatures originated from graphene phonons with wave vectors corresponding to the $\overline{K}$ and $\overline{K}'$ points of the surface Brillouin zone (BZ) [9] or various positions in reciprocal space [12]. At present, these observations may be substantiated by a phonon-mediated tunneling mechanism [9] where σ bands at $\overline{\Gamma}$ are mixed with π bands at $\overline{K}, \overline{K}'$ due to a graphene lattice that reflects the displacement patterns of $\overline{K}, \overline{K}'$ phonons [14].

Here, we report IETS performed with an STM on graphene-covered Ir(111). These investigations were motivated by the emerging picture that conveys high IET signals due to graphene phonons for quasifree graphene [9,11,12]. Unexpectedly, graphene on Ir(111) exhibits strong phonon signals, too. The signatures of various acoustic and optical graphene phonons with wave vectors comparable to the dimension of the BZ appear in IET spectra on wrinkles and blisters. We find that IET signals progressively increase with the height of the graphene nanostructures. Concomitantly, the spectroscopic signature of the Ir(111) surface resonance decreases with increasing graphene-metal separation. Moreover, decreasing the tip-graphene distance induces a gradual disappearance of the graphene phonon signatures from IET spectra. Model calculations capture the physics underlying these observations and highlight the role of phonon-mediated IET and the phonon density of states (DOS).

II. EXPERIMENT

Experiments were performed with an STM operated in ultrahigh vacuum (10^{-9} Pa) and at 6 K. The Ir(111) crystal was cleaned by Ar^+ bombardment and annealing. Graphene was prepared by thermal decomposition of C_2H_4 [15]. W tips were coated with a Au film by indentations into a Au substrate. A lock-in technique was used to detect the current response of the tunneling junction to a sinusoidal modulation of the bias voltage (10 mV_{rms}, 950 Hz). Wrinkles and blisters of graphene occur upon cooling the freshly prepared graphene sheet from elevated (>1400 K) to room temperature due to the mismatch in thermal expansion coefficients of graphene and Ir(111) [16].

III. RESULTS AND DISCUSSION

Figure 1(a) shows an overview STM image of graphene-covered Ir(111). Wrinkles and blisters are indicated by solid and dashed arrows, respectively. Wrinkles exhibit a wide distribution of lengths, widths, and apparent heights. Lengths (widths) as low as a few nanometers (a few tens of picometers) up to several hundreds of nanometers (a few nanometers) have been observed.

Remarkably, IET spectra acquired atop the highest elevation of wrinkles and blisters exhibit pronounced signatures [**2**, **3** in Fig. 1(b)], which are not observed on flat graphene [**1** in Fig. 1(b)]. Prominent signatures at ±57 and ±77 mV gradually increase with approaching the top of the graphene nanostructure. An additional rather broad spectroscopic feature is observed at ≈± 165 mV. Recently, phonon dispersion branches have experimentally been reported for graphene on Ir(111) [6,7]. The energy of the out-of-plane acoustic (ZA) phonon at $\overline{M}$ is $\hbar\omega(\mathrm{ZA},\overline{M}) = 58$ meV [$\hbar = h/(2\pi)$, where h is the Planck constant]. Transverse acoustic (TA) and out-of-plane optical (ZO) graphene phonons exhibit an energy of $\hbar\omega(\mathrm{TA},\overline{M}) \approx \hbar\omega(\mathrm{ZO},\overline{M}) = 77$ meV at $\overline{M}$. At $\overline{K}$, ZA and ZO phonons are degenerate with an energy of 65 meV. Longitudinal acoustic (LA) and optical (LO) as well as transverse optical (TO) phonon modes cover a broad energy range, 150 meV $\leqslant \hbar\Omega \leqslant$ 180 meV at $\overline{M}$ and $\overline{K}$. On the basis of these data [6,7] the peaks in d^2I/dV^2 spectra at ±57 mV may be assigned to graphene ZA phonons at $\overline{M}$. At ±77 mV

*nicolas.neel@tu-ilmenau.de

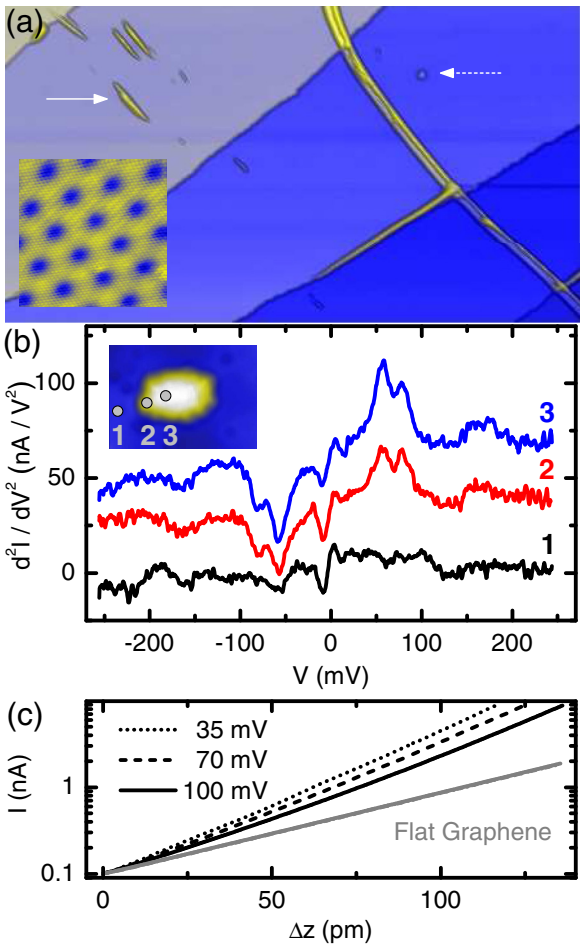

FIG. 1. (a) STM image of graphene-covered Ir(111) (0.1 nA, 100 mV, 350×190 nm^2). Arrows indicate wrinkles (solid) and blisters (dashed). Inset: Atomically resolved STM image of graphene (200 nA, 40 mV, 10×10 nm^2). (b) Spectra of d^2I/dV^2 acquired at locations indicated in the inset. Spectrum **2** (**3**) is shifted vertically by 30 nA/V^2 (60 nA/V^2). Feedback loop parameters: 0.1 nA, 250 mV. Inset: STM image of a blister (0.1 nA, 250 mV, 10×7 nm^2). (c) Tunneling current as a function of tip displacement acquired above a blister (black) and above flat graphene (gray). Feedback loop parameters: 0.1 nA and indicated bias voltages.

signatures of TA and ZO phonons at $\overline{M}$ may both contribute to the IET spectrum. The broad features centered at $\approx\pm$ 165 mV may be attributed to LA, LO, and TO graphene phonons at $\overline{M}$ and $\overline{K}$.

These assignments of peaks in d^2I/dV^2 spectra to graphene phonons are at odds with a previous study of graphene on SiO_2 where IET spectral features were rationalized in terms of ZA and ZO phonons at $\overline{K}$ [9]. In this seminal paper [9] a phonon-mediated inelastic tunneling mechanism was proposed to efficiently couple graphene σ bands at $\overline{\Gamma}$ with π bands at $\overline{K}$. This mechanism likewise explained the observed strong changes in dI/dV that are induced by the excitation of the graphene phonons. A more recent report presented IETS of graphene on top of hBN on SiO_2, where graphene phonons from large parts of the surface BZ were visible [12]. Indeed, in an extension of previous theoretical findings [14], we will show here that the band mixing process enhances the tunneling DOS at various graphene phonon energies.

Before entering into the theoretical discussion, Fig. 1(c) shows the evolution of the tunneling current with the variation of the tip-surface distance. The depicted data were acquired atop flat graphene (gray) and atop the highest point of a graphene blister (black). The indicated bias voltages ($V_1 =$ 35 mV, $V_2 = 70$ mV, $V_3 = 100$ mV) give rise to electron energies with $eV_1 < \hbar\omega(\mathrm{ZA},\overline{M}) < eV_2 < \hbar\omega(\mathrm{TA,ZO},\overline{M}) < eV_3 < \hbar\Omega$ (where e is the elementary charge). While on flat graphene the different data sets virtually coincide, the current evolution observed atop the blister depends on the bias voltage. Writing the tunneling current as $I \propto \exp(-\kappa\Delta z)$, the following decay constants κ are obtained for flat graphene ($\kappa \approx 2.2$ Å^{-1}), independent of the bias voltage, and for the graphene blister ($\kappa_1 \approx 3.7$ Å^{-1}, $\kappa_2 \approx 3.3$ Å^{-1}, $\kappa_3 \approx 2.9$ Å^{-1}). The observed decrease of the decay constant with increasing bias voltage is reminiscent of previously reported findings for graphene on SiO_2 [9]. For electron energies eV below the phonon excitation threshold, available graphene states for elastic tunneling are the π bands at $\overline{K}$ and $\overline{K}'$. Due to the wave-vector dependence of the decay constant (*vide infra*), the tunneling current decays fast with increasing tip-surface distance. When the electron energy surmounts the phonon excitation threshold, phonon-mediated tunneling with zero wave vector is allowed, which leads to a lower decay constant.

In the model the phonon-mediated coupling of π electrons at $\overline{K},\overline{K}'$ to states closer to the BZ center are considered. Only out-of-plane phonon modes, i.e., ZA and ZO phonons, enter into the calculations since they dominantly contribute to the spectroscopic features in the experimental spectra below 100 mV. The out-of-plane phonon branches are described by $H_{\mathrm{ph}} = \sum_{j,k} \hbar\omega_{j,k} a^\dagger_{j,k} a_{j,k}$, where $\hbar\omega_{j,k}$ denotes the energy of ZA, ZO graphene phonons and $a^\dagger_{j,k}$ ($a_{j,k}$) creates (annihilates) a ZA, ZO phonon. Graphene out-of-plane phonons mix π and nearly free σ bands. The π bands are described by $H_\pi = \sum_{\nu=\pm,q} \nu\varepsilon(q) c^\dagger_{\nu,q} c_{\nu,q}$ [$c^\dagger_{\nu,q}$ ($c_{\nu,q}$) creates (annihilates) an electron with momentum q, where $\varepsilon(q)$ is the energy of an electron state with momentum q]. The index $\nu = +$ ($\nu = -$) denotes the conduction (valence) band. Close to the Dirac points at $\overline{K}$ and $\overline{K}'$, i.e., at $\pm\mathbf{K} + \mathbf{Q}$ with $Q = |\mathbf{Q}| \ll |\mathbf{K}| = K$ and $\mathbf{K}$ being the wave vector at $\overline{K},\overline{K}'$ ($K = 1.7$ Å^{-1}), the electron energy may be approximated as $\varepsilon(Q) \approx \hbar v_{\mathrm{F}} Q$ (where v_{F} is the Fermi velocity). The nearly-free-electron states are considered as a flatband with energy E_σ, $H_\sigma = \sum_q d^\dagger_q E_\sigma d_q$, where $d^\dagger_q$ (d_q) creates (annihilates) an electron in the nearly free band with momentum q. The phonon-mediated band mixing reads $\Phi = \lambda_{\mathrm{eph}} \sum_{\nu,j,q,k} (d^\dagger_{k+q} c_{\nu,q} + c^\dagger_{\nu,k+q} d_q)(a_{j,k} + a^\dagger_{j,-k})$, where λ_{eph} is the electron-phonon coupling constant. A similar model was previously put forward [14] and is now generalized to describe phonons from the entire graphene BZ.

Within Tersoff-Hamann theory [17], the tunneling conductance is proportional to the local electron DOS at the position of the STM tip, which is typically at some height $z \gtrsim 3$–5 Å above the contact point. Thus, for each tunneling channel, the DOS inside the graphene sheet has to be weighted with the squared amplitude of the corresponding wave

function $|\Psi_{f,q}(z)|^2$ at height z. The inelastic contribution is given by

$$A^f(z,E) = \int_{\mathrm{BZ}} d^2q |\Psi_{f,q}(z)|^2 A^f(q,E), \tag{1}$$

where $A^f(q,E)$ is the momentum-resolved and energy-resolved spectral function of the nearly-free-electron states and follows the respective Green's function $G^f(q,E) = \langle\langle d_q^\dagger | d_q \rangle\rangle_E$ via $A^f(q,E) = -1/\pi\ \mathrm{Im}\, G^f(q,E)$.

In Eq. (1), the probability density $|\Psi_{f,q}(z)|^2 \propto \exp(-\kappa z)$ limits the part of the BZ that effectively contributes to the tunneling current due to the q dependence of the decay constant, $\kappa = 2\sqrt{\kappa_0^2 + q^2} \approx 2\kappa_0 + q^2/\kappa_0$. Significant contributions to the integral in Eq. (1) are thus limited to a range $q_\mathrm{m} < \sqrt{\kappa_0/z}$. With $\kappa_0 \approx 2.5$ Å^{-1}, $q_\mathrm{m} < 0.7$ Å^{-1} for $z = 5$ Å, $q_\mathrm{m} < 0.9$ Å^{-1} for $z = 3$ Å. Hence, virtual states from a disk $D_{q_\mathrm{m}}(\overline{\Gamma})$ of radius $q \lesssim q_\mathrm{m} \approx 0.7$–$0.9$ Å^{-1} around the BZ center contribute significantly to the inelastic tunneling. The effect of $|\Psi_{f,q}(z)|^2$ on the tunneling DOS can essentially be captured by limiting the integration in Eq. (1) to $A^f(z,E) = \int_{D_{q_\mathrm{m}}(\overline{\Gamma})} d^2q\, A^f(q,E)$.

The electron phonon coupling enters the Green's function $G^f(q,E) = 1/[E + i0^+ - E_\sigma - \Sigma(q,E)]$ via the self-energy $\Sigma(q,E)$. Since $E = eV \ll E_\sigma$, the spectral function simplifies to $A^f(q,E) \approx -\mathrm{Im}\,\Sigma(q,E)/(\pi E_\sigma^2) \propto \mathrm{Im}\,\Sigma(q,E)$. A direct generalization of the previously reported self-energy [14] yields in leading order of perturbation theory $\mathrm{Im}\,\Sigma(q,E) \approx -\pi\,\lambda_\mathrm{eph}^2 \sum_j \Theta(|E| - \hbar\omega_{j,\pm K+q}) N^\pi[E - \mathrm{sgn}(E)\hbar\omega_{j,\pm K+q}]$, where $N^\pi(E) \approx \alpha|E + \mu|$ with proportionality constant α is the linear DOS of the bare graphene π bands given for energies relative to the chemical potential μ. The resulting tunneling DOS is

$$\begin{aligned} A^f(z,E) &\propto \lambda_\mathrm{eph}^2 \int_{D_{q_\mathrm{m}}(\overline{\Gamma})} d^2q \sum_j \Theta(|E| - \hbar\omega_{j,\pm K+q}) \\ &\quad \times N^\pi[E - \mathrm{sgn}(E)\hbar\omega_{j,\pm K+q}] \\ &= \lambda_\mathrm{eph}^2 \int d\omega\, \Theta(|E| - \hbar\omega) \\ &\quad \times N^\pi[E - \mathrm{sgn}(E)\hbar\omega] N^{\mathrm{ph}*}(\hbar\omega), \end{aligned} \tag{2}$$

where the effective phonon DOS

$$N^{\mathrm{ph}*}(\hbar\omega) = \sum_j \int_{D_{q_\mathrm{m}}(\overline{K},\overline{K}')} d^2q\, \delta(\hbar\omega - \hbar\omega_{j,q}) \tag{3}$$

is restricted to phonon wave vectors in disks $D_{q_\mathrm{m}}(\overline{K},\overline{K}')$ of radius q_m around $\overline{K},\overline{K}'$. The tunneling DOS is thus a convolution of the graphene π band electronic DOS and the effective phonon DOS. The IETS signal is

$$\frac{d^2I}{dV^2} \propto \frac{dA^f(z,E)}{dE} \propto \mathrm{sgn}(E)\left[N^\pi(0)N^{\mathrm{ph}*}(|E|) + \alpha\lambda_\mathrm{eph}^2 \int_0^{|E|} d\omega\, N^{\mathrm{ph}*}(\hbar\omega)\right]. \tag{4}$$

If graphene is doped, i.e., $N^\pi \neq 0$ at $\mu = 0$ meV, peaks (dips) in the effective phonon DOS $N^{\mathrm{ph}*}(\hbar\omega)$ translate directly into peaks (dips) of the IETS signal.

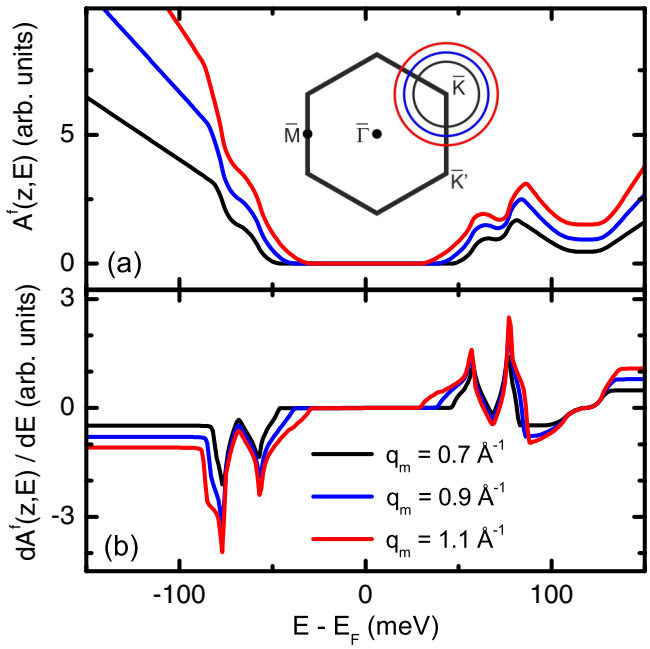

FIG. 2. Calculated tunneling DOS $A^f(z,E)$ (a) and IET spectra $dA^f(z,E)/dE$ (b) for indicated q_m and $\mu = -50$ meV. Inset: Graphene BZ with high symmetry points $\overline{K},\overline{K}',\overline{M}$. The concentric circles indicate the regions of the BZ that enter into the integration to obtain $A^f(z,E)$.

Figure 2 shows the calculated inelastic contribution to $A^f(z,E)$ [Fig. 2(a)] and $dA^f(z,E)/dE$ [Fig. 2(b)]. $\mu = -50$ meV was chosen, which is lower than μ of pristine graphene ($\mu = 0$ meV) and larger than μ of graphene on Ir(111) ($\mu = -100$ meV) [18]. The calculation of $A^f(z,E)$, Eq. (2), requires knowledge of $N^{\mathrm{ph}*}(\hbar\omega)$, Eq. (3), which was obtained from the dispersion of out-of-plane phonons in the next-nearest-neighbor approximation [19]. Force constants were adjusted such as to reproduce qualitatively correct dispersion relations between $\overline{M}$ and $\overline{K}$. For the numerical evaluation of Eq. (3), the δ function was approximated by a Lorentzian with a full width at half maximum of 5 meV. Since we were striving here for the qualitative evolution of the tunneling DOS, λ_eph and α in Eq. (4) were set to unity.

$A^f(z,E)$ curves appear with a gap around E_F symmetrically flanked by steplike increases at ± 58 meV (ZA) and ± 78 meV (ZO) [Fig. 2(a)], which give rise to dips and peaks in $dA^f(z.E)/dE$ [Fig. 2(b)], in agreement with the experimental observations. Deviating from previous results where only the signatures of graphene phonons at $\overline{K}$ were visible in IET spectra [9], Eq. (4) unveils that phonons at $\overline{M}$ with sufficiently high DOS may leave their fingerprint in the spectra as well. ZA and ZO phonons exhibit a rather flat dispersion around $\overline{M}$ in the $\overline{K}$-$\overline{M}$ direction. In particular, the dispersion exhibits saddle points at $\overline{M}$ with energies 58 and 78 meV [20]. These regions are partially covered by the disks $D_{q_\mathrm{m}}(\overline{K},\overline{K}')$ and thus give rise to peaks in $N^{\mathrm{ph}*}(\hbar\omega)$ at 58 and 78 meV.

The dips between these IETS peaks may be understood from $N^{\mathrm{ph}*}(\hbar\omega)$, too. Around $\overline{K}$ and $\overline{K}'$ the ZA and ZO phonon dispersion is linear and exhibits a conical point at ≈65 meV leading to the V-shaped minimum in $N^{\mathrm{ph}*}(\hbar\omega)$ and to the dips

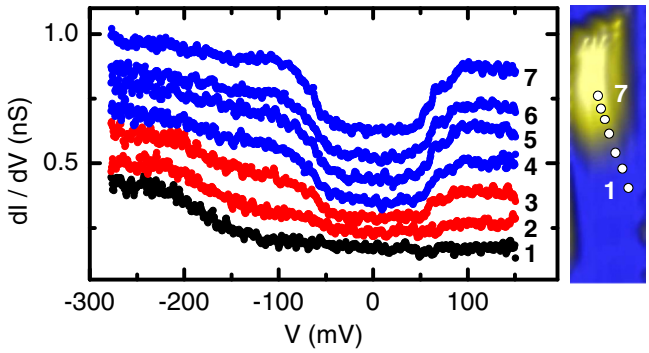

FIG. 3. Left: Spectra of dI/dV acquired at positions indicated in the STM image (right). Feedback loop parameters: 0.1 nA, −350 mV. Spectra **2**–**7** are consecutively offset by 0.1 nS. Right: STM image of a wrinkle (0.1 nA, −350 mV, 4 × 15 nm^2).

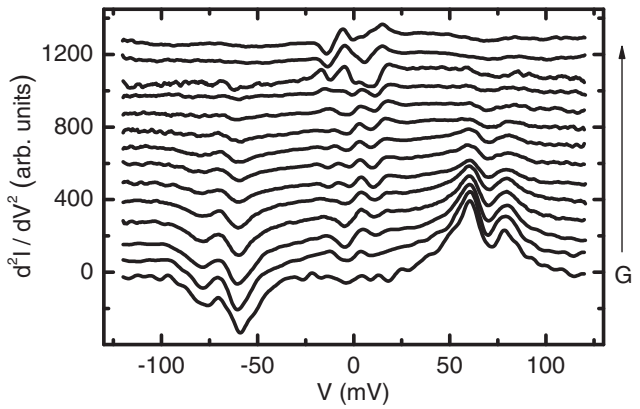

FIG. 4. d^2I/dV^2 spectra recorded above a wrinkle with increasing junction conductance G, which ranges from $5 \times 10^{-6} G_0$ (bottom) to $0.1 G_0$ (top). The spectra were normalized to the current at 120 mV and vertically offset.

in the IETS signals. Increasing q_m mainly broadens the steps (peaks and dips) in $A^f(z,E)$ $[dA^f(z,E)/dE]$ since phonons with larger wave vectors and different energies contribute to the IET process. Figure 2(a) likewise shows the signature of the Dirac point at ≈120 meV. Its absence from experimental spectra is presumably due to phonon features that cover the spectral range of the Dirac cone (*vide supra*).

In the remaining part of this Rapid Communication experimental evidence for the origin of the remarkable enhancement of phonon inelastic signals in IET spectra is presented. Figure 3 shows spatially resolved dI/dV spectra in the vicinity of a graphene wrinkle. Spectra acquired atop flat graphene (**1**) exhibit the signature of the holelike Ir(111) surface resonance [21,22] as a steplike feature at ≈− 170 mV. The resonance energy of clean Ir(111) is ≈− 300 meV with respect to E_F and is subject to a shift towards E_F on graphene-covered Ir(111) due to Pauli repulsion [23]. Upon approaching the top of the wrinkle (**2**–**7**) the surface resonance signature becomes gradually attenuated while the phonon-induced steplike increase of dI/dV at ±57 and ±77 mV is progressively enhanced. Spectra acquired at the top of the wrinkle do not show the Ir(111) surface resonance. This observation is indicative of a reduced graphene-Ir coupling for wrinkles and blisters. The surface resonance was previously reported to exhibit a high DOS at $\overline{\Gamma}$, which is associated with a high elastic tunneling current [23]. The spectra of Fig. 3 show that concomitantly with the progressive delamination of graphene the elastic electron tunneling due to the surface resonance is strongly reduced. In other words, IET dominates the evolution of dI/dV spectra and shows that wrinkles and blisters exhibit an electronic structure akin to genuine graphene [9,12]. It is noteworthy that for apparent heights of wrinkles and blisters ranging between 20 and 200 pm the IET signal was observed to still gradually increase. At the highest wrinkles and blisters (several nm of apparent height) inelastic tunneling was shown to increase dI/dV by a factor 60. Therefore, one may expect that with further delamination of graphene from Ir(111) the inelastic signal continues to be increased reflecting its further decoupling from the metal substrate.

The results presented in Fig. 3 unravel that in tunneling dI/dV spectra acquired atop graphene wrinkles and blisters the elastic electron tunneling is effectively suppressed while phonon-mediated IET leads to strong changes in dI/dV. Figure 4 demonstrates that this trend may be reversed, i.e., the inelastic signal becomes suppressed by enhancing the elastic contribution to the tunneling current. To this end, the junction conductance was successively increased and IET spectra were acquired atop a graphene wrinkle (Fig. 4). With increasing conductance (from bottom to top), that is, with closer proximity of the tip to the surface, the phonon spectroscopic signatures at ±57 and ±77 mV decrease. For junction conductances exceeding ≈$0.07 G_0$ ($G_0 = 2e^2/h$ is quantum of conductance)—which indicates a conductance in the contact range—they have essentially vanished from the spectra. The observed variation of the IET spectra with increasing junction conductance is compatible with the model proposed above. The lower tip-surface distance enlarges the elastic electron tunneling owing to the participation of electron states with a larger wave vector. In addition, close to and at contact the tip may be considered as a local defect that softens the in-plane momentum conservation and, concomitantly, locally lifts the suppression of inelastic electron tunneling [24].

IV. CONCLUSION

Wrinkles and blisters of graphene on a metal surface exhibit extraordinarily strong phonon signatures in IET spectra. Graphene out-of-plane acoustic and optical phonons at $\overline{M}$ and $\overline{K}$ contribute to the spectra. Due to the reduced graphene-metal hybridization in wrinkles and blisters, elastic electron tunneling is suppressed and IET is mediated by graphene phonons with a high DOS.

ACKNOWLEDGMENT

Financial support by the Deutsche Forschungsgemeinschaft through Grant No. KR 2912/10-1 and the research training group 2247 “Quantum Mechanical Materials Modelling” are acknowledged.

[1] A. C. Ferrari, J. C. Meyer, V. Scardaci, C. Casiraghi, M. Lazzeri, F. Mauri, S. Piscanec, D. Jiang, K. S. Novoselov, S. Roth, and A. K. Geim, Phys. Rev. Lett. **97**, 187401 (2006).
[2] A. C. Ferrari, Solid State Commun. **143**, 47 (2007).
[3] A. Politano, F. de Juan, G. Chiarello, and H. A. Fertig, Phys. Rev. Lett. **115**, 075504 (2015).
[4] L. Malard, M. Pimenta, G. Dresselhaus, and M. Dresselhaus, Phys. Rep. **473**, 51 (2009).
[5] A. Politano, A. R. Marino, V. Formoso, and G. Chiarello, Carbon **50**, 734 (2012).
[6] M. Endlich, A. Molina-Sánchez, L. Wirtz, and J. Kröger, Phys. Rev. B **88**, 205403 (2013).
[7] M. Endlich, H. P. C. Miranda, A. Molina-Sánchez, L. Wirtz, and J. Kröger, Ann. Phys. **526**, 372 (2014).
[8] V. W. Brar, Y. Zhang, Y. Yayon, T. Ohta, J. L. McChesney, A. Bostwick, E. Rotenberg, K. Horn, and M. F. Crommie, Appl. Phys. Lett. **91**, 122102 (2007).
[9] Y. Zhang, V. W. Brar, F. Wang, C. Girit, Y. Yayon, M. Panlasigui, A. Zettl, and M. F. Crommie, Nat. Phys. **4**, 627 (2008).
[10] V. W. Brar, S. Wickenburg, M. Panlasigui, C.-H. Park, T. O. Wehling, Y. Zhang, R. Decker, Ç. Girit, A. V. Balatsky, S. G. Louie, A. Zettl, and M. F. Crommie, Phys. Rev. Lett. **104**, 036805 (2010).
[11] R. Decker, Y. Wang, V. W. Brar, W. Regan, H.-Z. Tsai, Q. Wu, W. Gannett, A. Zettl, and M. F. Crommie, Nano Lett. **11**, 2291 (2011).
[12] F. D. Natterer, Y. Zhao, J. Wyrick, Y.-H. Chan, W.-Y. Ruan, M.-Y. Chou, K. Watanabe, T. Taniguchi, N. B. Zhitenev, and J. A. Stroscio, Phys. Rev. Lett. **114**, 245502 (2015).
[13] B. C. Stipe, M. A. Rezaei, and W. Ho, Science **280**, 1732 (1998).
[14] T. O. Wehling, I. Grigorenko, A. I. Lichtenstein, and A. V. Balatsky, Phys. Rev. Lett. **101**, 216803 (2008).
[15] H. Hattab, A. T. N'Diaye, D. Wall, G. Jnawali, J. Coraux, C. Busse, R. van Gastel, B. Poelsema, T. Michely, F.-J. M. zu Heringdorf, and M. H. von Hoegen, Appl. Phys. Lett. **98**, 141903 (2011).
[16] A. T. N'Diaye, R. van Gastel, A. J. Martínez-Galera, J. Coraux, H. Hattab, D. Wall, F.-J. Meyer zu Heringdorf, M. Horn-von Hoegen, J. M. Gómez-Rodrígez, B. Poelsema, C. Busse, and T. Michely, New J. Phys. **11**, 113056 (2009).
[17] J. Tersoff and D. R. Hamann, Phys. Rev. Lett. **50**, 1998 (1983).
[18] I. Pletikosić, M. Kralj, P. Pervan, R. Brako, J. Coraux, A. T. N'Diaye, C. Busse, and T. Michely, Phys. Rev. Lett. **102**, 056808 (2009).
[19] L. A. Falkovsky, J. Exp. Theor. Phys. **105**, 397 (2007).
[20] O. Dubay and G. Kresse, Phys. Rev. B **67**, 035401 (2003).
[21] J. F. van der Veen, F. J. Himpsel, and D. E. Eastman, Phys. Rev. B **22**, 4226 (1980).
[22] I. Pletikosić, M. Kralj, D. Šokčević, R. Brako, P. Lazić, and P. Pervan, J. Phys.: Condens. Matter **22**, 135006 (2010).
[23] S. J. Altenburg, J. Kröger, T. O. Wehling, B. Sachs, A. I. Lichtenstein, and R. Berndt, Phys. Rev. Lett. **108**, 206805 (2012).
[24] M. L. N. Palsgaard, N. P. Andersen, and M. Brandbyge, Phys. Rev. B **91**, 121403 (2015).